Published in final edited form as:
Sci Signal. ; 6(290): ra73. doi:10.1126/scisignal.2004184.

Activation of the Cl^- Channel ANO1 by Localized Calcium Signals in Nociceptive Sensory Neurons Requires Coupling with the IP_3 Receptor*

Xin Jin[1,2], **Shihab Shah**[1], **Yani Liu**[2], **Huiran Zhang**[2], **Meredith Lees**[1], **Zhaojun Fu**[1], **Jonathan D. Lippiat**[1], **David J. Beech**[1], **Asipu Sivaprasadarao**[1], **Stephen A. Baldwin**[1], **Hailin Zhang**[2], and **Nikita Gamper**[1,2,*]

[1]Faculty of Biological Sciences, School of Biomedical Sciences, University of Leeds, Leeds, UK

[2]Department of Pharmacology, Hebei Medical University, Shijiazhuang, China

Abstract

We report that ANO1 (also known as TMEM16A) Ca^{2+}-activated Cl^- channels in small neurons from dorsal root ganglia are preferentially activated by particular pools of intracellular Ca^{2+}. These ANO1 channels can be selectively activated by the G protein-coupled receptor (GPCR)-induced release of Ca^{2+} from intracellular stores, but not by Ca^{2+} influx through voltage-gated Ca^{2+} channels. This ability to discriminate between Ca^{2+} pools was achieved by the tethering of ANO1-containing plasma membrane domains, which also contained GPCRs such as bradykinin receptor-2 and protease-activated receptor-2, to juxtamembrane regions of the endoplasmic reticulum. Interaction of the C-terminus and the first intracellular loop of ANO1 with IP_3R1 (inositol 1,4,5-trisphosphate receptor 1) contributed to the tethering. Disruption of membrane microdomains blocked the ANO1 and IP_3R1 interaction and resulted in the loss of coupling between GPCR signaling and ANO1. The junctional signaling complex enabled ANO1-mediated excitation in response to specific Ca^{2+} signals rather than to global changes in intracellular Ca^{2+}.

Introduction

Ca^{2+}-activated Cl^- channels (CaCCs) are an important group of ion channels with diverse physiological roles. They are involved in regulation of epithelial transport, smooth muscle contraction, neuronal excitability, and sensory transduction (1). CaCCs are present in many mammalian sensory cells, including olfactory neurons (2, 3), photosensitive rods and cones (4, 5), and dorsal root ganglia (DRG) neurons (6, 7). The molecular identity of CaCCs remained enigmatic until 2008 when members of a new family of anion channels, the

*To whom correspondence should be addressed: Nikita Gamper, Faculty of Biological Sciences, University of Leeds, LS2 9JT Leeds, UK, Tel: +44 113 3437923, n.gamper@leeds.ac.uk.

Author contributions: XJ, NG, SAB, AS, HaZ planned experiments; XJ, NG, SS, YL, HuZ, ML, ZF, performed experiments; XJ, NG, SAB, AS, HuZ, JDL, DJB, SS, YL, HaZ, ML, YL analyzed data; NG (aided by all other authors) wrote manuscript.

Competing interests: Authors declare that no conflict of interests exists.

Europe PMC Funders Author Manuscripts

anoctamin (ANO) or TMEM16 proteins, were identified as likely candidates (8-10). In particular, ANO1 (TMEM16A) mediates CaCC currents in epithelial and smooth muscle cells (11-14) and in damage-sensing (nociceptive or 'pain') DRG neurons (6, 7), whereas ANO2 (TMEM16B) mediates CaCC currents in the cilia of olfactory sensory neurons (15, 16). Although there is a consensus that ANO1 and ANO2 are CaCCs, it is not clear if other members of the family share the same function. For example, ANO6 (TMEM16F) has been reported to be a Cl^- channel (17), a nonselective cation channel (18), and a phospholipid scramblase (19). In addition, the yeast ANO ortholog, which is most similar to mammalian ANO10, localizes to the endoplasmic reticulum (ER) and links together ER and plasma membranes at ER-PM junctions in yeast (20).

Because smooth muscles and sensory neurons have high intracellular Cl^- concentrations, activation of CaCCs in these cells causes depolarization and is excitatory. There are many different pathways in these cells through which intracellular Ca^{2+} may increase, including electrical activity itself. To control cellular excitability, a mechanism is required to ensure selective coupling of CaCCs to the appropriate physiological Ca^{2+} signal. Peripheral nociceptive neurons are normally silent and fire action potentials (APs) only in response to potentially damaging mechanical, thermal, or chemical stimuli, but not in response to innocuous stimuli. Therefore, these neurons must be able to identify Ca^{2+} signals originating specifically from the potentially damaging stimulus. We found that ANO1 may represent one of the mechanisms for distinguishing intracellular Ca^{2+} signals.

One mechanism to activate CaCC is through activation of voltage-gated calcium channels (VGCCs) (21); however, one study found that only 50% of all DRG neurons exhibit a CaCC current in response to activation of VGCCs (22). Furthermore, subdivision of neurons into large (mostly mechanosensitive), medium (mostly myelinated Aδ nociceptors) and small (mostly unmyelinated C nociceptors) revealed that the medium and large neurons exhibit VGCC-coupled CaCC currents (23-25), but this is rare in the small neurons (6, 24, 25). Instead, in nociceptive DRG neurons, ANO1 is activated following the release of Ca^{2+} from inositol trisphosphate (IP_3)-sensitive ER stores induced by the inflammatory mediator bradykinin (BK) (6). Such CaCC currents depolarize these neurons and trigger APs capable of generating painful sensations. Here, we found that the coupling of ANO1 activation in nociceptive DRG neurons to release of Ca^{2+} form intracellular stores was achieved by coupling the channel to specific membrane microdomains that occurred at sites where the plasma membrane and ER were adjacent.

Results

ANO1 in nociceptive neurons is activated by Ca^{2+} released from intracellular stores but not by Ca^{2+} influx through VGCC

Because CaCC currents were rarely activated by VGCC-mediated signals and instead were activated by Ca^{2+} released from IP_3-sensitive ER stores in nociceptive DRG neurons, we hypothesized that this preference for a particular source of intracellular Ca^{2+} may represent a mechanism ensuring the selectivity and fidelity of signal transduction mediated by DRG neurons. Consistent with previous reports (6, 23, 24), we found by whole-cell patch clamp recording that, in the majority (19/20, 95%) of small DRG neurons from rats, VGCC

activation with a voltage stimulus did not result in CaCC activation (Fig. 1A). In these experiments, we used a double-pulse protocol in which two 500-ms depolarizing pulses to 0 mV and to +80 mV were given in succession from a holding potential of −80 mV. Both pulses result in activation of VGCC but only first pulse allows substantial Ca^{2+} influx through VGCC, because at +80 mV the driving force for Ca^{2+} is diminished. The outward current observed during the second voltage pulse was not a VGCC-mediated Ca^{2+} current because it was not blocked by the VGCC blocker Cd^{2+} (Fig. 1A, green trace). In neurons that did respond with CaCC current, the CaCC current was calculated as a difference in peak tail current amplitudes after each of the depolarizing pulses with and without Ca^{2+} influx (6, 24, 25); we considered neurons displaying less than 40 pA of such current as not displaying activation of CaCC by VGCC. We restricted our analysis to the small-diameter, TRPV1-positive neurons, which were identified by the exposure to 1 μM capsaicin at the end of the recording (Fig. 1A, inset); most of such neurons also have the BK receptor B_2R (6, 26).

Ca^{2+} activation of ANO1 is voltage-dependent (27), exhibiting an increased sensitivity at depolarizing potentials. For example, if at −80 mV the EC_{50} for ANO1 activation by Ca^{2+} is in the range of 3 μM, this parameter at depolarizing voltages is much lower (~500 nM at voltages above +50 mV) (27). Thus, it is possible that at more positive voltages activation of VGCC may deliver enough Ca^{2+} to activate CaCC. We used voltage ramps from −80 to +80 mV (fig. S1) delivered with 1 s intervals between the ramps to facilitate use-dependent inactivation of VGCC and measured the currents. Recordings were made with a NMDG-chloride-based extracellular solution containing 2 mM $CaCl_2$ and a CsCl-based pipette solution. VGCC were activated in the expected voltage window (an inward ‘hump’ of the voltage trace) peaking at 0 to +10 mV, as expected for N and P/Q channels underlying the majority of VGCC current in DRG (28). Recurrent application of the voltage ramp caused rapid rundown of VGCC current, such that the inward Ca^{2+} current almost completely disappeared by 5^{th} to 7^{th} sweep (fig. S1A, B). We then compared the amplitude of the outward current at +80 mV between the first sweep (VGCC are active) and the 5^{th}-7^{th} sweep (VGCC are inactivated). The peak outward current amplitude at +80 mV was not affected by the inactivation of VGCC (fig. S1A, C), suggesting that even at +80 mV VGCC failed to activate CaCC.

In sharp contrast with the poor efficiency of VGCC for activating CaCC in small DRG neurons, stimulation of pro-inflammatory B_2R or protease-activated receptor 2 (PAR-2) resulted in prominent CaCC currents in many of these neurons: BK (Fig. 1B) and the synthetic peptide ligand PAR2-PL (Fig. 1C; Table 1) activated CaCC, producing inward currents, in 16/35 (46%) and 8/15 (53%) of TRPV1-positive DRG neurons, respectively. We tested whether the cells that exhibited a CaCC response to GPCR stimulation would respond to VGCC with a CaCC response by applying the VGCC double-pulse protocol and GPCR ligand in succession to the same small DRG neuron. In neurons in which PAR2-PL and BK induced inward currents of 145 ± 47 pA and 259 ± 158 pA, respectively, VGCC activation failed to induce any measurable CaCC (fig. S1D).

Previously, we demonstrated that BK-induced Cl^- current was sensitive to CaCC blockers, niflumic acid (NFA), 5-nitro-2-(3-phenylpropylamino)benzoic acid (NPPB), and 4,4′-diisothiocyanatostilbene-2, 2′-disulphonic acid (DIDS) (6). Since a more specific ANO1

blocker, T16A-A01, has been identified (29, 30), we tested if BK-induced current in DRG is also sensitive to T16A-A01 and found that T16A-A01 inhibited BK-induced current by 88 ± 6% (fig. S1E). Activation of CaCC by BK in small DRG neurons depends on ER Ca^{2+} release and is blocked by the IP_3R inhibitor Xestospongin C and by depletion of ER Ca^{2+} with thapsigargin (6). However, these experiments did not rule out store-operated Ca^{2+} entry as a potential source of CaCC activation. Here, we performed a patch-clamp experiment in which extracellular Ca^{2+} was briefly omitted to block store-operated Ca^{2+} entry (Fig. 1B). Under such conditions BK still induced inward current in 5/10 neurons with a peak amplitude of 187 ± 49 pA, which was not significantly different from control (159 ± 19 pA; Fig. 1D), indicating that store-operated Ca^{2+} entry was not necessary and that the BK-induced CaCC was activated by Ca^{2+} released from the ER. PAR-2 receptor signaling is similar to that of B_2R in DRG neurons (6, 31). Consistent with PAR-2 mediating CaCC through Ca^{2+} released from the ER, the inward currents induced by PAR2-PL were inhibited by the Cl^- channel blocker NFA and by ER Ca^{2+} depletion with thapsigargin (Fig. 1C, E).

Coexpression of exogenous ANO1 with B_2R in HEK293 cells resulted in BK-induced currents with properties similar to those of BK-induced currents in DRG neurons (fig. S2). Bath application of BK in cells transfected with both ANO1 and B_2R (fig. S2A, B), but not in cells expressing only B_2R (fig. S2C), or intracellular dialysis of 600 nM free Ca^{2+} through the patch pipette (fig. S2D) induced an outwardly-rectifying current that reversed near 0 mV in HEK293 cells. Similar currents were reversibly induced by BK in DRG neurons (fig. S2E, F). These recordings were made using extracellular and intracellular solutions with equal Cl^- concentrations and with Na^+ and K^+ substituted by the impermeable cations TEA^+ and Cs^+, respectively.

These electrophysiological recordings suggested that CaCC in small DRG neurons was activated by GPCR-induced ER Ca^{2+} release but not by the Ca^{2+} influx through VGCC. To confirm this finding with an alternative technique, we performed fluorescent imaging of intracellular iodide with the halide-sensitive H148Q/I152L EYFP mutant (32). ANO1 is highly permeable to I^- ions (1) and H148Q/I152L EYFP fluorescence is quenched by I^-. Perfusion of DRG neurons transiently transfected with H148Q/I152L EYFP with external solution in which 30 mM NaCl was substituted by 30 mM NaI induced a slow decrease in fluorescence (Fig. 2A, B). Subsequent application of BK induced a robust quenching of H148Q/I152L EYFP fluorescence in ~50% of transfected neurons (Fig. 2A, B). Because the rate of H148Q/I152L EYFP quenching was variable (probably due to various background anion permeability pathways), we co-applied 30 mM NaI-containing bath solution with other drugs and averaged the resulting fluorescence response of all neurons for the entire time series (Fig. 2B). In control neurons (vehicle, NaI only) the fluorescence [expressed as fluorescence intensity (F) normalized to the basal level at t = 0 (F_0)] decreased from unity to 0.76 ± 0.05 over the 300 s of application; BK induced a significantly greater reduction to 0.53 ± 0.04. The effect of BK was blocked by NFA (Fig. 2B). However, depolarization of DRG neurons with 50 mM KCl (depolarization to ~-25 mV according to the Nernst equation) to activate VGCC did not result in a significantly greater rundown of fluorescence than that seen in control neurons. Nevertheless, fluorescent Ca^{2+} imaging experiments confirmed that 50 mM KCl application consistently produced global intracellular Ca^{2+}

increases with amplitudes comparable to those produced by BK (fig. S3A, B). Thus, imaging experiments confirmed poor coupling of CaCC to VGCC in DRG neurons.

Localized Ca^{2+} signals for ANO1 activation are formed within junctional microdomains bridging the plasma membrane and ER

In DRG neurons both B_2R and PAR-2 are coupled to $G_{q/11}$ G proteins, which activate phospholipase C leading to IP_3 generation and robust ER Ca^{2+} release (6, 26, 31). Moreover, junctional microdomains bringing together B_2R in the plasma membrane and IP_3R in the ER have been reported in sympathetic neurons (33, 34). We hypothesized that a preferential coupling of ANO1 channels to GPCR-induced Ca^{2+} release from the ER as opposed to Ca^{2+} entering the cytosol through VGCCs may result from the close juxtaposition of plasma membrane GPCRs and ANO1 channels with ER Ca^{2+} release sites, and the absence of such a proximity between ANO1 and VGCCs. Such an arrangement, in combination with the reportedly low Ca^{2+} sensitivity of ANO1 [EC_{50} ~2-5 μM at negative voltages (8-10, 27)], could potentially render ANO1 insensitive to 'global' increases in Ca^{2+} concentration. Sensitivity to 'local' and 'global' Ca^{2+} signals can be probed with two Ca^{2+} buffers that differ in their Ca^{2+} binding kinetics but have similar Ca^{2+} affinity: EGTA is a 'slow' Ca^{2+} buffer that cannot block fast local increases in Ca^{2+} and BAPTA is a 'fast' buffer that blocks both local and global Ca^{2+} signals (35, 36). This paradigm has been used to probe the proximity of ANO2 to VGCC and NMDA receptors in hippocampal neurons (21) and of endogenous CaCC to VGCC and ryanodine receptors in avian DRG (37); we utilized the same approach here to investigate whether the activation of ANO1 by B_2R or PAR-2 required local Ca^{2+} signaling. PAR-2-induced CaCC currents occurred in 5/7 neurons dialyzed with EGTA to block global Ca^{2+} signals (Fig. 3A). The amplitude of PAR-2-induced CaCC (at −60 mV) in EGTA-dialyzed neurons was 215.4 ± 11.2 pA and was not significantly different from control neurons with 176.5 ± 16.2 pA. In contrast, BAPTA abolished PAR-2-induced currents almost completely with only 1/9 neurons displaying a small CaCC current (Fig.3A), suggesting that local Ca^{2+} signaling was necessary for ANO1 activation and that ANO1 was close to ER Ca^{2+} release sites.

DRG neurons primarily have IP_3R1 (38); therefore, we performed immunoprecipitation and Western blotting using lysates from freshly extracted rat DRG to investigate whether IP_3R1 and ANO1 interact. ANO1 coprecipitated from DRG lysates with an antibody against IP_3R1 (Fig. 3B) and, reciprocally, IP_3R1 coprecipitated with an antibody against ANO1 (Fig. 3C). Specificity of the antibody against ANO1 was verified using human umbilical vein endothelial cells (HUVECs), which do not express detectable *Ano1* (as tested by RT-PCR; fig. S4A). No band at the predicted molecular weight of ANO1 (~114 kD) was detected in the lysate of non-transfected HUVECs or in the IP_3R1 immunoprecipitates; but was detected in HUVECs transfected with *Ano1* cDNA (fig. S4B). ANO1 was not detected in DRG lysates immunoprecipitated with an antibody against sarco-endoplasmic reticulum calcium ATPase (SERCA) (fig. S4C). IP_3R1 immunoprecipitates also contained both B_2R and PAR-2 (Fig. 3D), suggesting that IP_3R1, ANO1, and these GPCRs may be in a complex.

Lipid rafts serve as sites for the assembly of signaling complexes (39) and B_2R may localize to lipid rafts in DRG (40, 41). Therefore, we hypothesized that ANO1 and the GPCRs that

regulate it may be assembled in a microdomain within a lipid raft or an analogous structure and this membrane microdomain is tethered to the juxtaposed ER region by some means; the IP_3R-ANO1 interaction could contribute to such tethering. Consistent with a role for lipid rafts in organizing this signaling complex, we detected B_2R and PAR-2 in immunoprecipitates of the lipid raft marker caveolin-1(42) (Cav-1) (Fig. 3E).

To confirm the coimmunoprecipitation results, we used a fluorescent proximity ligation assay (PLA), which detects two proteins that are closer than 30 nm (43) (Fig. 4A; see Material and Methods). We confirmed the specificity and effectiveness of the antibody against ANO1 for labelling the protein in cells by showing that the antibody only produced a signal in HUVECs transfected with *Ano1* cDNA but did not stain nontransfected HUVECs (fig. S4D). In DRG cultures ANO1 stained neurons but not glia (fig. S4E). The IP_3R1 antibody labelled reticular structures in DRG neurons (fig. S4E). With PLA for ANO1 and IP_3R1, we detected punctate fluorescent signals with characteristic puncta diameter of ~1 μm (44) in small DRG neurons but not in glia (Fig 4B); whereas no PLA puncta were detected in nontransfected HUVECs (Fig. 4C). A pan-VGCC antibody (binds to all VGCC's α1 subunits) robustly stained DRG neurons but not glia (fig. S4E); however, no PLA puncta were detected with PLA for ANO1 and VGCC in DRG neurons (Fig. 4D). Thus, ANO1 and IP_3R1 were within ~30 nm at specific sites within small DRG neurons, whereas no such proximity between ANO1 and VGCC could be detected.

To confirm that ANO1 and the GPCRs were present in lipid rafts, we performed density gradient fractionation of whole DRG lysates and found that ANO1, B_2R, PAR-2, and Cav-1 were present in the same fractions (Fig. 5A, upper panel); whereas the non-raft marker, transferrin receptor (CD71) (42), localized to heavier membrane fractions. Cholesterol depletion with methyl-β-cyclodextrin (βMCD), which disrupts lipid rafts (45), resulted in redistribution of Cav-1, ANO1, and some of the GPCRs to heavier membrane fractions (Fig. 5A, lower panel). Furthermore, βMCD treatment significantly decreased the coimmunoprecipitation of IP_3R1 by ANO1 (Fig. 5B), suggesting that the lipid raft environment may be necessary to support the proximity of the ANO1 and IP_3R1. Coimmunoprecipitation of B_2R by IP_3R1 was somewhat reduced by βMCD treatment but this did not reach significance (Fig. 5B); perhaps the interaction between the B_2R and IP_3R1 in this complex have different dependency on the lipid raft environment compared to that of ANO1 and IP_3R1. With PLA, βMCD treatment significantly reduced the number of puncta in PLA-positive neurons (Fig. 5C), indicating that the ANO1 and IP_3R1 complex was disrupted.

To identify the regions within ANO1 and IP_3R1 that interacted, we constructed three glutathione-*S*-transferase (GST)-fusion proteins, each containing one of the largest predicted cytosolic domains of ANO1 (Fig. 6A): the C- and N-terminal hydrophilic regions and the loop between the second and third predicted transmembrane domains (TM2-3). GST pull-down experiments performed with whole DRG lysates revealed that the C-terminus and the TM2-3 loop, but not the N-terminus, of ANO1 precipitated IP_3R1 (Fig. 6A, lower right panel). We next subcloned these three cytosolic regions of ANO1 into bicistronic pIRES-EGFP vector and overexpressed these individually in DRG neurons. Patch-clamp recordings revealed that overexpression of either the TM2-3 loop or the C-terminus of ANO1 abolished

the PAR2-PL-induced inward current, whereas overexpression of the N-terminal domain resulted in PAR2-PL-induced currents that were not significantly different from vector-only control (Fig. 6B-D). Thus, we proposed that the TM2-3 loop or the C-terminus disrupted the native ANO1-IP_3R1 coupling and interfered with ANO1 activation.

Together these data suggested the existence of CaCC signaling complexes in DRG neurons that consists of (i) a plasma membrane component containing ANO1 and B_2R or PAR-2 or both in a cholesterol- and Cav-1-enriched microdomain; and (ii) a juxtaposed ER region containing IP_3R1. The interactions between ANO1 and the IP_3R1 (mediated by the C-terminus and the TM2-3 loop of ANO1) contribute to linking the two membranes, which is required for CaCC activation by the GPCRs.

ANO1-containing microdomains underlie fidelity of Ca^{2+} signaling in nociceptive neurons

To determine if the plasma membrane-ER structure was important for mediating CaCC selectivity for local Ca^{2+} signals, we examined the effect of cholesterol extraction with βMCD on the ability of global Ca^{2+} signals mediated by VGCCs to induce CaCC. Whereas in the control group only 1/20 neurons displayed CaCC currents in response to VGCC activity; significantly more of the βMCD-treated group 10/20 (50%) displayed VGCC-triggered CaCC currents (Fig. 7A, B, Table 1). The amplitude of the VGCC current was not affected by the βMCD treatment (580 ± 85 pA in control compared to 522 ± 62 pA in βMCD-treated group). Likewise, Ca^{2+} transients induced in DRG neurons by depolarization with 50 mM KCl also were not affected by βMCD treatment (fig. S3B). Treatment of the neurons with the βMCD analog α-cyclodextrin (αCD), which cannot sequester cholesterol (46), did not significantly change the coupling of CaCCs to VGCCs; the proportion of neurons in which Ca^{2+} influx through VGCCs induced CaCC tail currents (1/21 or 5%) was not different from that seen with untreated neurons and was significantly lower than such proportion in the βMCD-treated group (Fig. 7B, Table 1). We confirmed the activation of CaCC by global Ca^{2+} signals with the H148Q/I152L EYFP imaging approach. In βMCD-treated neurons, NaI alone caused a decrease in F/F_0 from unity to 0.77 ± 0.05 (Fig. 7C), which was not different from the decrease observed in control, βMCD-untreated neurons (Fig. 2B; a decrease of F/F_0 to 0.76 ± 0.05). However, depolarization with 50 mM KCl induced a significantly greater decrease in fluorescence in βMCD-treated neurons as compared with untreated cells. Thus, in βMCD-treated cells 50 mM KCl induced a decrease of F/F_0 to 0.46 ± 0.03 (Fig. 7C) versus a decrease to 0.69 ± 0.03 in control cells (Fig. 2B and 7C).

As an indication of the physiological importance of the junctional microdomain, we tested if disruption of the junctional microdomain affected the excitability of DRG neurons. In accord with previous observations (6, 26), in response to 600 pA of depolarizing current injection most control DRG neurons (18/21) fired a single AP and only 3 neurons fired multiple APs (Fig. 7D, E). In contrast, after the βMCD treatment half of the neurons (11/22) fired multiple APs (Fig. 7D, E). When βMCD-treated neurons were recorded under conditions in which intracellular Cl^- was replaced with acetate (and, thus, Cl^- channel opening would result in hyperpolarization, not depolarization), only 3/19 neurons fired multiple APs, indicating that no increase in the proportion of hyperexcitable neurons

occurred (Fig. 7E, Table 1). Likewise, αCD treatment also did not increase the proportion of excitable neurons (Fig. 7E, Table 1).

Although βMCD treatment enhanced coupling of CaCC to VGCC, the opposite occurred for the coupling of CaCC to GPCR. Thus, after βMCD treatment, neither BK nor PAR2-PL induced CaCC activation in the majority of DRG neurons tested (Fig. 7F, G; Table 1). Treatment of the neurons with the αCD did not prevent the responses to BK and PAR2-PL (Fig. 7F, G; Table 1) because 50% of the neurons responded to BK and PAR2-PL with inward currents of 236 ± 48 and 254 ± 52 pA, respectively. Ca^{2+} imaging revealed that after βMCD treatment BK induced Ca^{2+} transients in DRG neurons (fig. S3B; Table 1); the transients were slightly (but not significantly) delayed and reduced. Even though BK still induced Ca^{2+} release, we propose that lipid raft disruption caused a disturbance to the ANO1 signaling complex (Fig. 7H) such that the ER Ca^{2+} release sites were no longer close enough to the low-Ca^{2+}-affinity ANO1 channels to supply a sufficient amount of Ca^{2+} to activate the channel. In turn, some delocalized ANO1 channels gain proximity to VGCCs (both of these channels reside within the plasma membrane) when lipid rafts are disrupted and become susceptible to activation following VGCC opening.

Discussion

Our study demonstrated that the ANO1 (CaCC) in small nociceptive DRG neurons exists as a part of a signaling complex that also harbors GPCRs responsive to inflammatory mediators (Fig. 7H). The plasma membrane component of the complex was tethered to the ER; the interactions of the C-terminus and the TM2-3 loop of ANO1 with the IP_3R1 contributed to the tethering, which may also involve further scaffolding proteins. Such assembly not only ensures the activation of the poorly Ca^{2+}-sensitive ANO1 by inflammatory mediator-induced Ca^{2+} release from the stores but also protects the ANO1 channels from promiscuous activation by Ca^{2+} influx through VGCCs, thus preventing an unwarranted positive feedback loop of CaCC-induced depolarization in response to the global Ca^{2+} influx following an AP. It is also conceivable that ANO1-containing microdomains create a local environment that is poorly accessible for cytosolic Ca^{2+} ions that do not originate from the ER, thus protecting ANO1 (CaCC) from any ‘irrelevant’ Ca^{2+} source. The latter property of the ANO1-containing signaling microdomain can be particularly important in light of the recently reported temperature sensitivity of ANO1 (7). Indeed, ANO1 appears to be intrinsically heat sensitive (activation threshold ~44 °C) and, a rise in intracellular Ca^{2+} lowers the temperature threshold for ANO1 activation below the normal body temperature. Activation of ANO1 by heat contributes to the excitation of peripheral nociceptive terminals and, thus, to generation of nociceptive signals and pain (7). In such a scenario, a mechanism protecting ANO1 from global Ca^{2+} signals in nociceptive neuronss is indeed necessary, as otherwise these neurons would become hypersensitive to heat every time the intracellular Ca^{2+} became elevated. Interestingly, CaCC in medium and large DRG neurons is apparently different from that of small nociceptive neurons: It is coupled to VGCC (24) but is reportedly mediated by another Cl^- channel, Best1 (23, 25). In hippocampal neurons, CaCC is also coupled to VGCC but, again, it was found to be mediated not by ANO1 but by ANO2 channel (21). Thus, there is likely to be a high degree of specificity among various CaCC channels in the way these couple to intracellular Ca^{2+} sources.

Similar ANO1 signaling complexes may exist in other neurons and non-neuronal cells. For example, in smooth muscle cells a close association of endogenous CaCCs and ryanodine receptors has been hypothesized (47). In smooth muscle myocytes, ANO1 localizes to lipid rafts and disruption of lipid rafts by βMCD results in the increased activation of ANO1-mediated currents by voltage at high intracellular calcium concentrations (0.5 μM) (48). Because Ca^{2+} facilitates the voltage-sensitivity of ANO1 (49), it is conceivable that lipid raft disruption in smooth muscle myocytes exposes ANO1 to global Ca^{2+}, thus making the channels more easily activated by voltage. Thus, similarly to nociceptive neurons, microdomains in smooth muscle cells may play a dual role, providing a mechanism for specific coupling of ANO1 to intracellular stores and protecting them from global changes in cytosolic Ca^{2+} concentration.

In summary, our data put forward the existence of specific signaling structures bringing together ANO1, GPCRs, and ER-localized IP_3 receptors. These structures may serve to ensure the fidelity of acute inflammatory signals in nociceptive DRG neurons and may also exist in other cell types.

Materials and Methods

Cell culture and transfection

DRG were extracted from all spinal levels of 21 day old Wistar rats and neurons were dissociated and cultured as described (31). No growth factors were added to the culture media (DMEM supplemented with GlutaMAX I (Invitrogen), 10% fetal bovine serum, penicillin (50 U/ml), and streptomycin (50 μg/ml). DRG cultures were transfected using Nucleofector (Lonza) as described previously (50). HUVECs were cultured as described previously (51) and transfected using FuGENE HD (Promega) according to the manufacturer's instructions. HEK293 cells were cultured as described previously (52) and transfected using Lipofectamine 2000 (Invitrogen) according to the manufacturer's instructions. Vectors: pGEX-KT (GE Healthcare) was used to generate GST-fusion ANO1 fragments; pIRES-EGFP (Clontech) was used to transfect these fragments into DRG neurons as free peptides; the sequence of pEYFP-N1 (Clontech) was altered using Quikchange (Stratagene) to generate H148Q/I152L YFP variant (32), which was then subcloned into pcDNA6-V5/His vector (Invitrogen); mouse ANO1 was overexpressed in HEK293 and HUVEC cells in pEGFP-N1 (Clontech).

Electrophysiology

Whole cell patch clamp and current clamp recordings were performed as described in (6). In whole cell patch clamp experiments with the activation of CaCCs by GPCRs, the internal pipette solution contained (in mM): 150 CsCl, 5 $MgCl_2$, 1 K_2ATP, 0.1 NaGTP, 1 EGTA, 10 HEPES (pH 7.4 with CsOH). In Ca^{2+} clamping experiments the internal solution contained (in mM): 135 CsCl, 5 $MgCl_2$, 5 HEPES, 1 K_2ATP, 0.1 NaGTP, and 10 mM of either EGTA or BAPTA, pH 7.35 with CsOH. In all intracellular solutions, intracellular free Ca^{2+} was adjusted to 100 nM using the Maxchelator program (Stanford University). The external solution contained (in mM): 145 TEACl, 2 $CaCl_2$, 10 mM HEPES (pH 7.4 with CsOH). In a 'Ca^{2+}-free' external solution $CaCl_2$ was omitted and 1 mM EGTA was added to chelate

residual free Ca^{2+}. CaCC activation by GPCRs was measured by continuous recording at −60 mV; CaCC activation by VGCC was measured using extracellular solution containing (in mM): 155 TEACl, 1 $CaCl_2$, 0.5 $MgCl_2$, 10 HEPES (adjusted to pH 7.35 with CsOH). Where indicated, 155 mM NMDG chloride was used instead of TEA. Replacement of Na^+ and K^+ in the extra- and intracellular solutions was made to minimize the contribution of Na^+ and K^+ channels. CaCC activation was measured as inward tail current following a 500 ms square pulse to 0 mV from the holding potential of −80 mV with a subsequent second 500 ms pulse to +80 mV, which caused negligible Ca^{2+} fluxes due to the diminished driving force. Sampling rate was 200 Hz. CaCC amplitude was calculated as a difference in peak tail current amplitudes after the depolarizing pulses with and without Ca^{2+} influx. VGCC current displayed variable run-down so the CaCC current amplitude was calculated from the first sweep. In recordings with voltage ramp protocols (BK-induced CaCC), the external solution contained (in mM): 155 TEACl, 2 $CaCl_2$, 0.1 $CdCl_2$, 10 HEPES (pH 7.4 with CsOH). In recordings with voltage ramp protocols (VGCC-induced CaCC), the external solution contained (in mM): 140 NMDG, 2 $CaCl_2$, 1.5 $MgCl_2$, 10 HEPES, 10 glucose (pH 7.4 with HCl); the internal solution contained (in mM): 150 CsCl, 5 MgCl2, 10 HEPES (pH 7.4 with CsOH); supplemented with amphotericin B (400 μg/ml). Current clamp experiments were performed in whole cell mode with extracellular solution containing (in mM): 160 NaCl, 2.5 KCl, 2 $CaCl_2$, 1 $MgCl_2$, 10 HEPES (pH 7.4 with NaOH); intracellular solution contained (in mM): 150 KCl, 5 $MgCl_2$, 1 K_2ATP, 0.1 NaGTP, 1 EGTA, 10 HEPES. In a 'low $[Cl^-]_i$' pipette solution 140 mM KCl was replaced by equimolar K-acetate. PAR2-PL is a peptide SLIGRL-NH_2 (Santa Cruz); BK was from Sigma-Aldrich. Inward current amplitudes are given as absolute values (unless indicated otherwise).

Fluorescent imaging

H148Q/I152L YFP fluorescence was recorded using a Nikon Swept Field confocal microscope equipped with a 488 nm argon laser, an EM-CCD camera and controlled by the NIS Elements 3.2 software (Nikon). The extracellular solution for these experiments contained (in mM): 160 NaCl, 2.5 KCl, 2 $CaCl_2$, 1 $MgCl_2$, 10 HEPES (pH 7.4 with NaOH). To induce iodide influx 30 mM NaCl was replaced with 30 mM NaI. Ca^{2+} imaging was performed as described previously (6, 26); briefly, neurons were loaded with fluo-4 AM (2 μM) in the presence of Pluronic F-127 (0.02%). DRG cultures were treated with 10 mM βMCD or vehicle for 45 min during the loading with fluo-4 AM and imaged immediately using a Nikon TE2000E microscope in epi-fluorescence mode.

Immunoprecipitation and Western blotting

The procedures were performed as described previously (53). Briefly, DRG (from all levels) from 21 day old Wistar rats were homogenized in non-denaturing lysis buffer (20 mM Tris HCl pH 8.0, 137 mM NaCl, 10% glycerol, 1% Triton X-100, 2 mM EDTA) with protease and phosphatase inhibitors (Roche) and incubated for 2 h at 4 °C, before centrifugation for 20 min/13,000*g*. The supernatant was incubated overnight at 4°C with antibody (0.5-1.5 μg). On the following day protein G sepharose beads (GE Healthcare, London, UK) were added and incubation continued at 4 °C under rotary agitation for 4 h; beads were washed four times with lysis buffer (with inhibitors) and centrifuged and the supernatants discarded. For Western blot analysis, total DRG lysates, immunoprecipitates, or membrane fractions were

boiled for 5 min in SDS–polyacrylamide gel electrophoresis (PAGE) sample buffer (50 mM Tris-HCl, pH 6.8, containing 5% 2-mercaptoethanol, 10% glycerol, and 1% SDS) and analyzed by SDS-PAGE, followed by transfer to PVDF membrane by electroblotting. The membranes were incubated in blocking buffer (TBS containing 5% skimmed milk powder and 0.1% Tween-20) for 2 h, followed by incubation with primary antibody, diluted in the same buffer, at 4 °C overnight. The membranes were washed in TBS containing 0.1% Tween-20 before incubation with an appropriate secondary (horseradish peroxidase-conjugated anti-IgG or IRDye®-conjugated anti-IgG). Bound antibodies were detected using the SuperSignal chemiluminescence system (ECL, Thermo) or an Odyssey 9120 Infrared Imaging System (LI-COR, Lincoln, NE). For βMCD treatment whole ganglia lysates were incubated with 50 mM βMCD for 1 h at 37 °C. In co-immunoprecipitation experiments 5% of total lysate protein was run on the same gel for input control. The following antibodies were used in this study: goat antibody against TMEM16A (sc-69343, lot #F2812; Santa Cruz), mouse antibody against CD71 (Santa Cruz), rabbit antibody against IP_3R1 (Cell Signaling), mouse antibody against B_2R (BD Biosciences), mouse antibody against caveolin-1(BD Biosciences); mouse antibody against PAR-2 (Santa Cruz); mouse antibody against GST (Santa Cruz); mouse antibody against SERCA isoforms 1 and 2 (Badrilla Ltd); rabbit antibody against calcium channel (α1 Subunit), pan (Sigma); mouse antibody against GFAP (Sigma).

Proximity ligation assay

The PLA (Duolink, Onlink Bioscience) was performed according to manufacturer's instructions. In this technique the proteins within a sample are labelled with specific antibodies and then treated with PLA probes, which are secondary antibodies conjugated with short DNA strands. If two proteins are colocalized within less than 30 nm of each other, the two DNA probes are ligated, a unique new DNA sequence is amplified and a color reaction developed. DRG cultures were fixed and permeabilized with acetone:methanol (1:1) for 20 min at −20°C. After incubation with primary antibodies, cultures were incubated with corresponding PLA probes (antibody against goat PLUS, antibody against rabbit MINUS PLA probes) for 1 h at 37°C, and ligation was performed using the DuoLink II Detection Reagents Kit (Green). The amplification and detection were performed according to the manufacturer's instructions. The primary antibodies used were the same as in immunoprecipitation experiments. Confocal images were taken with an LSM510 META microscope (Zeiss).

Lipid raft isolation

The procedures were performed as described previously (54). All steps were carried out at 4 °C. DRG were isolated from 21 day old Wistar rats (5 rats per one preparation) and frozen at −80 °C until use. Lipid rafts were isolated by sucrose gradient centrifugation. Briefly, frozen DRG tissue was thawed and homogenized using a glass Potter-Elvehjem homogenizer in 1.5 ml MBST buffer (50 mM MES, 150 mM NaCl, pH 6.5, 1% Triton X-100, 5 μg/ml leupeptin, 5 μg/ml aprotinin, and 2 μg/ml pepstatin A). The homogenate was then mixed with 1.5 ml of 85% sucrose in MBS buffer (50 mM MES, 150 mM NaCl, pH 6.5, 5 μg/ml leupeptin, 5 μg/ml aprotinin, and 2 μg/ml pepstatin A) before overlaying successively with 3 ml volumes of 35% sucrose in MBS buffer and 5% sucrose in MBS buffer. For lipid raft

isolation, the resultant gradients were ultracentrifuged (100,000*g*, 18 h, 4 °C), and 9 fractions were collected from each (from the top to the bottom of the tube, fractions 1–9). Samples were analyzed by SDS-PAGE followed by Western blotting. All independent experiments within the data series were treated identically and repeated at least three times.

GST pull-down assays

The procedures were performed as described previously (55, 56). Briefly, regions encoding the rat ANO1 (UniProt accession D4A915) N-terminus (residues 1-407), TM2-3 loop (505-568), and C-terminus (963-1040) were PCR cloned from rat DRG cDNA and subcloned into the vector pGEX-KT. Constructs were produced in *Escherichia coli* strain BL21-gold cells (Stratagene) and purified with Glutathione Sepharose 4B beads (GE Healthcare, London, U.K.) at 4 °C overnight with gentle rotation. For GST pulldowns, rat DRG were homogenized in non-denaturing lysis buffer (20 mM Tris HCl pH 8.0, containing 137 mM NaCl, 10% glycerol, 1% Triton X-100, and 2 mM EDTA) with protease and phosphatase inhibitors and incubated for 2 h at 4 °C. Insoluble debris was removed by centrifugation for 20 min/13,000*g*. GST protein and GST fusion proteins (bound to Glutathione Sepharose, GE Healthcare, London, UK) were incubated with rat DRG tissue homogenate overnight at 4°C. The beads were washed and bound proteins were eluted in SDS-PAGE sample buffer, and analyzed by western blotting.

Statistics

All data are given as mean ± SEM; unless indicated otherwise, only values from responsive cells are included into the mean values. Differences between groups were assessed by Student's *t* test; the differences were considered significant at $p \leq 0.05$. χ squared test was used to determine whether there were differences in the number of cells responding to a treatment.

Supplementary Material

Refer to Web version on PubMed Central for supplementary material.

Acknowledgments

We thank Prof. Jim Deuchars, Drs Sarah. C. Callaghan and Zhanfeng Zhang for advice on the experimental design, Katarzyna Marszalek and Honling Rong for technical assistance, Dr. Jing Li for HUVECs and Dr. Louisa Pettinger for help with Ca^{2+} imaging.

Funding: This work was supported by grants from Wellcome Trust and MRC to NG, DJB and AS and grants from the National Natural Science Foundation of China (31270882) and National Basic Research Program (013CB531302) to HaZ. NG and HaZ received international joint project grant from Royal Society (JP080524) and National Science Foundation of China (30911130137).

References and Notes

1. Huang F, Wong X, Jan LY. International Union of Basic and Clinical Pharmacology. LXXXV: calcium-activated chloride channels. Pharmacol. Rev. 2012; 64:1. [PubMed: 22090471]
2. Kleene SJ, Gesteland RC. Calcium-activated chloride conductance in frog olfactory cilia. J. Neurosci. 1991; 11:3624. [PubMed: 1941099]

3. Lowe G, Gold GH. Nonlinear amplification by calcium-dependent chloride channels in olfactory receptor cells. Nature. 1993; 366:283. [PubMed: 8232590]
4. Barnes S, Hille B. Ionic channels of the inner segment of tiger salamander cone photoreceptors. J. Gen. Physiol. 1989; 94:719. [PubMed: 2482325]
5. Maricq AV, Korenbrot JI. Calcium and calcium-dependent chloride currents generate action potentials in solitary cone photoreceptors. Neuron. 1988; 1:503. [PubMed: 2483100]
6. Liu B, Linley JE, Du X, Zhang X, Ooi L, Zhang H, Gamper N. The acute nociceptive signals induced by bradykinin in rat sensory neurons are mediated by inhibition of M-type K^+ channels and activation of Ca^{2+}-activated Cl^- channels. J. Clin. Invest. 2010; 120:1240. [PubMed: 20335661]
7. Cho H, Yang YD, Lee J, Lee B, Kim T, Jang Y, Back SK, Na HS, Harfe BD, Wang F, Raouf R, Wood JN, Oh U. The calcium-activated chloride channel anoctamin 1 acts as a heat sensor in nociceptive neurons. Nat. Neurosci. 2012; 15:1015. [PubMed: 22634729]
8. Caputo A, Caci E, Ferrera L, Pedemonte N, Barsanti C, Sondo E, Pfeffer U, Ravazzolo R, Zegarra-Moran O, Galietta LJ. TMEM16A, a membrane protein associated with calcium-dependent chloride channel activity. Science. 2008; 322:590. [PubMed: 18772398]
9. Schroeder BC, Cheng T, Jan YN, Jan LY. Expression cloning of TMEM16A as a calcium-activated chloride channel subunit. Cell. 2008; 134:1019. [PubMed: 18805094]
10. Yang YD, Cho H, Koo JY, Tak MH, Cho Y, Shim WS, Park SP, Lee J, Lee B, Kim BM, Raouf R, Shin YK, Oh U. TMEM16A confers receptor-activated calcium-dependent chloride conductance. Nature. 2008; 455:1210. [PubMed: 18724360]
11. Huang F, Rock JR, Harfe BD, Cheng T, Huang X, Jan YN, Jan LY. Studies on expression and function of the TMEM16A calcium-activated chloride channel. Proc. Natl. Acad. Sci. U. S. A. 2009; 106:21413. [PubMed: 19965375]
12. Rock JR, O'Neal WK, Gabriel SE, Randell SH, Harfe BD, Boucher RC, Grubb BR. Transmembrane protein 16A (TMEM16A) is a Ca^{2+}-regulated Cl^- secretory channel in mouse airways. J Biol Chem. 2009; 284:14875. [PubMed: 19363029]
13. Davis AJ, Forrest AS, Jepps TA, Valencik ML, Wiwchar M, Singer CA, Sones WR, Greenwood IA, Leblanc N. Expression profile and protein translation of TMEM16A in murine smooth muscle. Am. J. Physiol. Cell Physiol. 2010; 299:C948. [PubMed: 20686072]
14. Manoury B, Tamuleviciute A, Tammaro P. TMEM16A/anoctamin 1 protein mediates calcium-activated chloride currents in pulmonary arterial smooth muscle cells. J. Physiol. 2010; 588:2305. [PubMed: 20421283]
15. Billig GM, Pal B, Fidzinski P, Jentsch TJ. Ca^{2+}-activated Cl^- currents are dispensable for olfaction. Nat .Neurosci. 2011; 14:763. [PubMed: 21516098]
16. Stephan AB, Shum EY, Hirsh S, Cygnar KD, Reisert J, Zhao H. ANO2 is the cilial calcium-activated chloride channel that may mediate olfactory amplification. Proc. Natl. Acad. Sci. U. S. A. 2009; 106:11776. [PubMed: 19561302]
17. Tian Y, Schreiber R, Kunzelmann K. Anoctamins are a family of Ca^{2+}-activated Cl^- channels. J. Cell. Sci. 2012; 125:4991. [PubMed: 22946059]
18. Yang H, Kim A, David T, Palmer D, Jin T, Tien J, Huang F, Cheng T, Coughlin SR, Jan YN, Jan LY. TMEM16F forms a Ca^{2+}-activated cation channel required for lipid scrambling in platelets during blood coagulation. Cell. 2012; 151:111. [PubMed: 23021219]
19. Suzuki J, Umeda M, Sims PJ, Nagata S. Calcium-dependent phospholipid scrambling by TMEM16F. Nature. 2010; 468:834. [PubMed: 21107324]
20. Manford AG, Stefan CJ, Yuan HL, Macgurn JA, Emr SD. ER-to-Plasma Membrane Tethering Proteins Regulate Cell Signaling and ER Morphology. Dev. Cell. 2012; 23:1129. [PubMed: 23237950]
21. Huang WC, Xiao S, Huang F, Harfe BD, Jan YN, Jan LY. Calcium-Activated Chloride Channels (CaCCs) Regulate Action Potential and Synaptic Response in Hippocampal Neurons. Neuron. 2012; 74:179. [PubMed: 22500639]
22. Mayer ML. A calcium-activated chloride current generates the after-depolarization of rat sensory neurones in culture. J. Physiol. 1985; 364:217. [PubMed: 2411915]
23. Boudes M, Sar C, Menigoz A, Hilaire C, Pequignot MO, Kozlenkov A, Marmorstein A, Carroll P, Valmier J, Scamps F. Best1 is a gene regulated by nerve injury and required for Ca^{2+}-activated Cl-

current expression in axotomized sensory neurons. J. Neurosci. 2009; 29:10063. [PubMed: 19675239]

24. Andre S, Boukhaddaoui H, Campo B, Al-Jumaily M, Mayeux V, Greuet D, Valmier J, Scamps F. Axotomy-induced expression of calcium-activated chloride current in subpopulations of mouse dorsal root ganglion neurons. J. Neurophysiol. 2003; 90:3764. [PubMed: 12944538]
25. Boudes M, Scamps F. Calcium-activated chloride current expression in axotomized sensory neurons: what for? Front. Mol. Neurosci. 2012; 5:35. [PubMed: 22461766]
26. Linley JE, Ooi L, Pettinger L, Kirton H, Boyle JP, Peers C, Gamper N. Reactive oxygen species are second messengers of neurokinin signaling in peripheral sensory neurons. Proc. Natl. Acad. Sci. U. S. A. 2012; 109:E1578. [PubMed: 22586118]
27. Xiao Q, Yu K, Perez-Cornejo P, Cui Y, Arreola J, Hartzell HC. Voltage- and calcium-dependent gating of TMEM16A/Ano1 chloride channels are physically coupled by the first intracellular loop. Proc. Natl. Acad. Sci. U. S. A. 2011; 108:8891. [PubMed: 21555582]
28. Rola R, Szulczyk PJ, Witkowski G. Voltage-dependent Ca^{2+} currents in rat cardiac dorsal root ganglion neurons. Brain Res. 2003; 961:171. [PubMed: 12535791]
29. Namkung W, Phuan PW, Verkman AS. TMEM16A inhibitors reveal TMEM16A as a minor component of calcium-activated chloride channel conductance in airway and intestinal epithelial cells. J. Biol. Chem. 2011; 286:2365. [PubMed: 21084298]
30. Davis AJ, Shi J, Pritchard HA, Chadha PS, Leblanc N, Vasilikostas G, Yao Z, Verkman AS, Albert AP, Greenwood IA. Potent vasorelaxant activity of the TMEM16A inhibitor T16A(inh)-A01. Br. J. Pharmacol. 2013; 168:773. [PubMed: 22946562]
31. Linley JE, Rose K, Patil M, Robertson B, Akopian AN, Gamper N. Inhibition of M current in sensory neurons by exogenous proteases: a signaling pathway mediating inflammatory nociception. J. Neurosci. 2008; 28:11240. [PubMed: 18971466]
32. Galietta LJ, Haggie PM, Verkman AS. Green fluorescent protein-based halide indicators with improved chloride and iodide affinities. FEBS Lett. 2001; 499:220. [PubMed: 11423120]
33. Delmas P, Brown DA. Junctional signaling microdomains: bridging the gap between the neuronal cell surface and Ca^{2+} stores. Neuron. 2002; 36:787. [PubMed: 12467583]
34. Delmas P, Wanaverbecq N, Abogadie FC, Mistry M, Brown DA. Signaling microdomains define the specificity of receptor-mediated $InsP_3$ pathways in neurons. Neuron. 2002; 34:209. [PubMed: 11970863]
35. Augustine GJ, Santamaria F, Tanaka K. Local calcium signaling in neurons. Neuron. 2003; 40:331. [PubMed: 14556712]
36. Berkefeld H, Sailer CA, Bildl W, Rohde V, Thumfart JO, Eble S, Klugbauer N, Reisinger E, Bischofberger J, Oliver D, Knaus HG, Schulte U, Fakler B. BKCa-Cav channel complexes mediate rapid and localized Ca^{2+}-activated K^+ signaling. Science. 2006; 314:615. [PubMed: 17068255]
37. Ward SM, Kenyon JL. The spatial relationship between Ca^{2+} channels and Ca^{2+}-activated channels and the function of Ca^{2+}-buffering in avian sensory neurons. Cell Calcium. 2000; 28:233. [PubMed: 11032779]
38. Dent MA, Raisman G, Lai FA. Expression of type 1 inositol 1,4,5-trisphosphate receptor during axogenesis and synaptic contact in the central and peripheral nervous system of developing rat. Development. 1996; 122:1029. [PubMed: 8631248]
39. Lingwood D, Simons K. Lipid rafts as a membrane-organizing principle. Science. 2010; 327:46. [PubMed: 20044567]
40. Jeske NA, Berg KA, Cousins JC, Ferro ES, Clarke WP, Glucksman MJ, Roberts JL. Modulation of bradykinin signaling by EP24.15 and EP24.16 in cultured trigeminal ganglia. J. Neurochem. 2006; 97:13. [PubMed: 16515556]
41. Jeske NA. Somatosensory scaffolding structures. Front. Mol. Neurosci. 2012; 5:2. [PubMed: 22291616]
42. Liu L, Pilch PF. A critical role of cavin (polymerase I and transcript release factor) in caveolae formation and organization. J. Biol. Chem. 2008; 283:4314. [PubMed: 18056712]
43. Soderberg O, Gullberg M, Jarvius M, Ridderstrale K, Leuchowius KJ, Jarvius J, Wester K, Hydbring P, Bahram F, Larsson LG, Landegren U. Direct observation of individual endogenous

protein complexes in situ by proximity ligation. Nature Methods. 2006; 3:995. [PubMed: 17072308]

44. Jarvius J, Melin J, Goransson J, Stenberg J, Fredriksson S, Gonzalez-Rey C, Bertilsson S, Nilsson M. Digital quantification using amplified single-molecule detection. Nature Methods. 2006; 3:725. [PubMed: 16929318]
45. Maekawa S, Sato C, Kitajima K, Funatsu N, Kumanogoh H, Sokawa Y. Cholesterol-dependent localization of NAP-22 on a neuronal membrane microdomain (raft). J. Biol. Chem. 1999; 274:21369. [PubMed: 10409698]
46. Ohtani Y, Irie T, Uekama K, Fukunaga K, Pitha J. Differential effects of alpha-, beta- and gamma-cyclodextrins on human erythrocytes. Eur. J. Biochem. 1989; 186:17. [PubMed: 2598927]
47. Bao R, Lifshitz LM, Tuft RA, Bellve K, Fogarty KE, ZhuGe R. A close association of RyRs with highly dense clusters of Ca^{2+}-activated Cl^{-} channels underlies the activation of STICs by Ca^{2+} sparks in mouse airway smooth muscle. J. Gen. Physiol. 2008; 132:145. [PubMed: 18591421]
48. Sones WR, Davis AJ, Leblanc N, Greenwood IA. Cholesterol depletion alters amplitude and pharmacology of vascular calcium-activated chloride channels. Cardiovasc. Res. 2010; 87:476. [PubMed: 20172862]
49. Yu K, Duran C, Qu Z, Cui YY, Hartzell HC. Explaining calcium-dependent gating of anoctamin-1 chloride channels requires a revised topology. Circ. Res. 2012; 110:990. [PubMed: 22394518]
50. Kirton HM, Pettinger L, Gamper N. Transient overexpression of genes in neurons using nucleofection. Methods Mol. Biol. 2013; 998:55. [PubMed: 23529420]
51. Li J, Cubbon RM, Wilson LA, Amer MS, McKeown L, Hou B, Majeed Y, Tumova S, Seymour VA, Taylor H, Stacey M, O'Regan D, Foster R, Porter KE, Kearney MT, Beech DJ. Orai1 and CRAC channel dependence of VEGF-activated Ca^{2+} entry and endothelial tube formation. Circ. Res. 2011; 108:1190. [PubMed: 21441136]
52. Jia Q, Jia Z, Zhao Z, Liu B, Liang H, Zhang H. Activation of epidermal growth factor receptor inhibits KCNQ2/3 current through two distinct pathways: membrane PtdIns(4,5)P_2 hydrolysis and channel phosphorylation. J. Neurosci. 2007; 27:2503. [PubMed: 17344388]
53. Jin X, Song X, Li L, Wang Z, Tao Y, Deng L, Tang M, Yi W, Cao Y. Blockade of AP-1 activity by dominant-negative TAM67 can abrogate the oncogenic phenotype in latent membrane protein 1-positive human nasopharyngeal carcinoma. Mol. Carcinog. 2007; 46:901. [PubMed: 17477349]
54. Persaud-Sawin DA, Lightcap S, Harry GJ. Isolation of rafts from mouse brain tissue by a detergent-free method. J. Lipid Res. 2009; 50:759. [PubMed: 19060326]
55. Anderson D, Mehaffey WH, Iftinca M, Rehak R, Engbers JD, Hameed S, Zamponi GW, Turner RW. Regulation of neuronal activity by Cav3-Kv4 channel signaling complexes. Nat. Neurosci. 2010; 13:333. [PubMed: 20154682]
56. Singh H, Warburton S, Vondriska TM, Khakh BS. Proteomics to identify proteins interacting with P2X2 ligand-gated cation channels. J. Vis. Exp. 2009; 27:1178. [PubMed: 19455095]

Europe PMC Funders Author Manuscripts

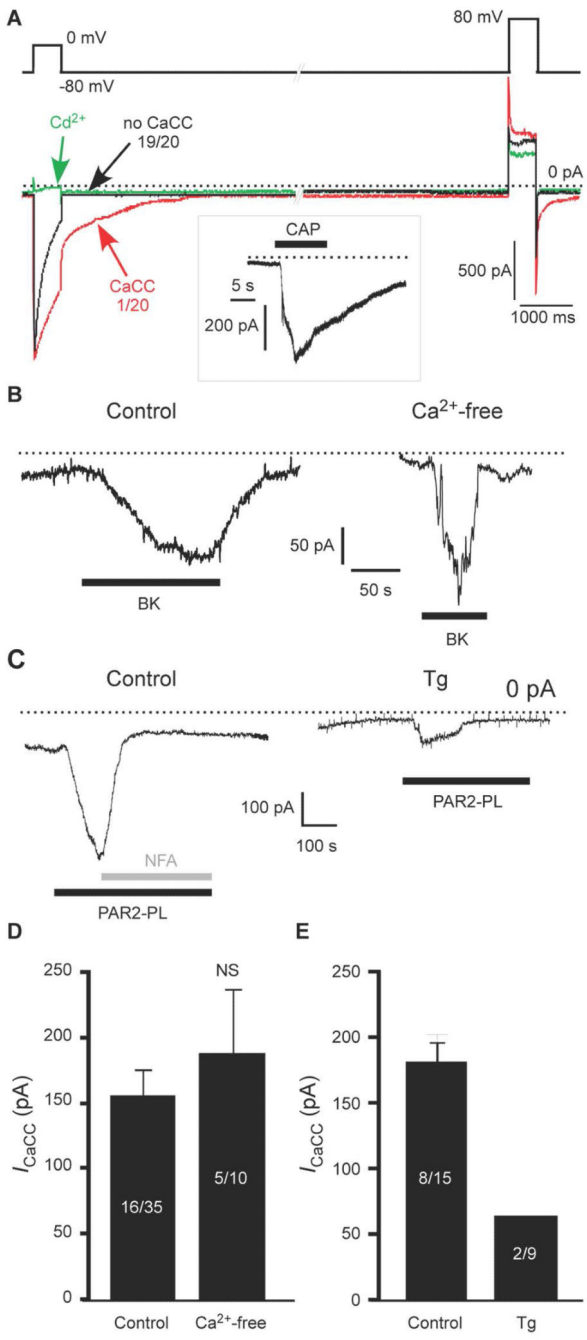

Fig. 1. Ca^{2+}-activated Cl^- channels in small DRG neurons are preferentially activated by Ca^{2+} release from the ER

(A) Whole cell patch-clamp recording of currents in response to a voltage pulse from −80 to 0 mV in small DRG neurons. The recordings were made using TEACl-based extracellular and CsCl-based intracellular solutions. The green trace represents inhibition of VGCC by Cd^{2+} (100 μM) in the same cell in which the control (black) trace was recorded. The box inset depicts the response of the same cell to capsaicin (CAP; 1 μM) at a holding potential of −60 mV. 19/20 and 1/20 represent the number of neurons exhibiting the specified type of

response. (**B**) BK (1 μM)-induced inward current in a small DRG neuron when recorded in extracellular solution with and without Ca^{2+}. (**C)** PAR2-PL (10 μM)-induced inward current in a small DRG neuron; in control conditions or following pretreatment with thapsigargin (Tg, 2 μM, 3 min); NFA, niflumic acid (100 μM). (**D, E)** Summary data for (B) and (C), respectively. Number of responsive neurons out of total neurons tested is indicated within each bar.

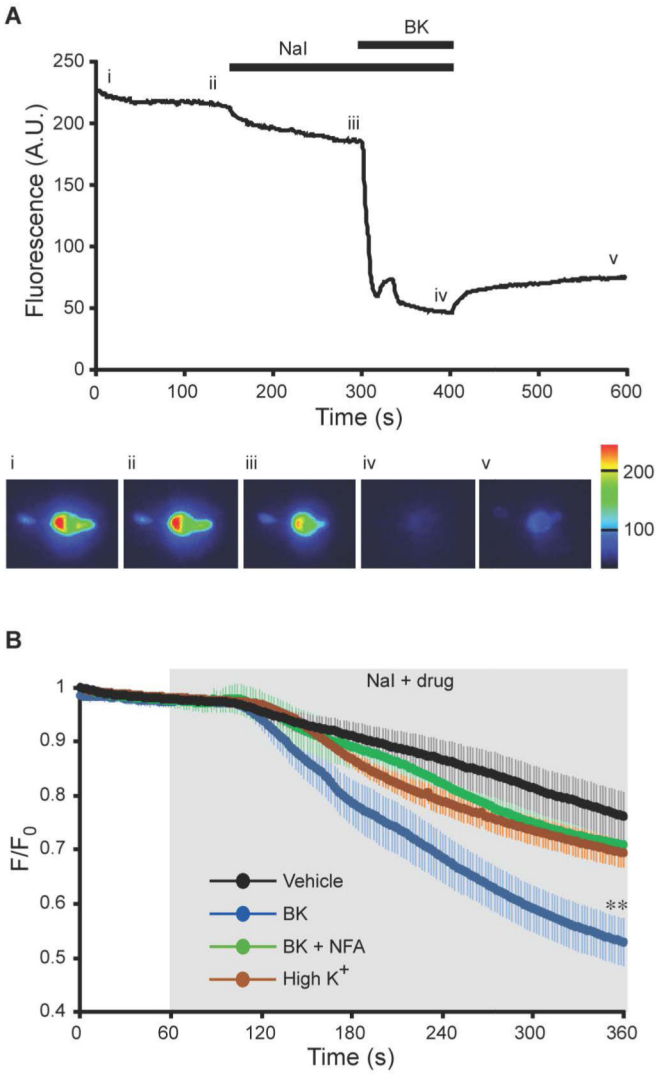

Fig. 2. Imaging CaCC activation with a halide-sensitive EYFP

(A) Fluorescence intensity of a DRG neuron transfected with H148Q/I152L EYFP was monitored during application of bath solution containing 30 mM NaI on its own or in combination with 1 μM BK (as indicated by the black bars). Pseudocolored images (lower panel) were taken at times indicated by the Roman numerals. **(B)** Averaged time courses of normalized fluorescence (F/F_0) of H148Q/I152L EYFP-transfected neurons perfused with 30 mM NaI-containing extracellular solution either alone (n = 10) or in combination with 1 μM BK (n = 15); with 1 μM BK and 100 μM NFA (n = 8); or with 50 mM KCl (n = 27). The time of compound application is indicated by the shaded area. ** $p \leq 0.01$ as compared to vehicle alone.

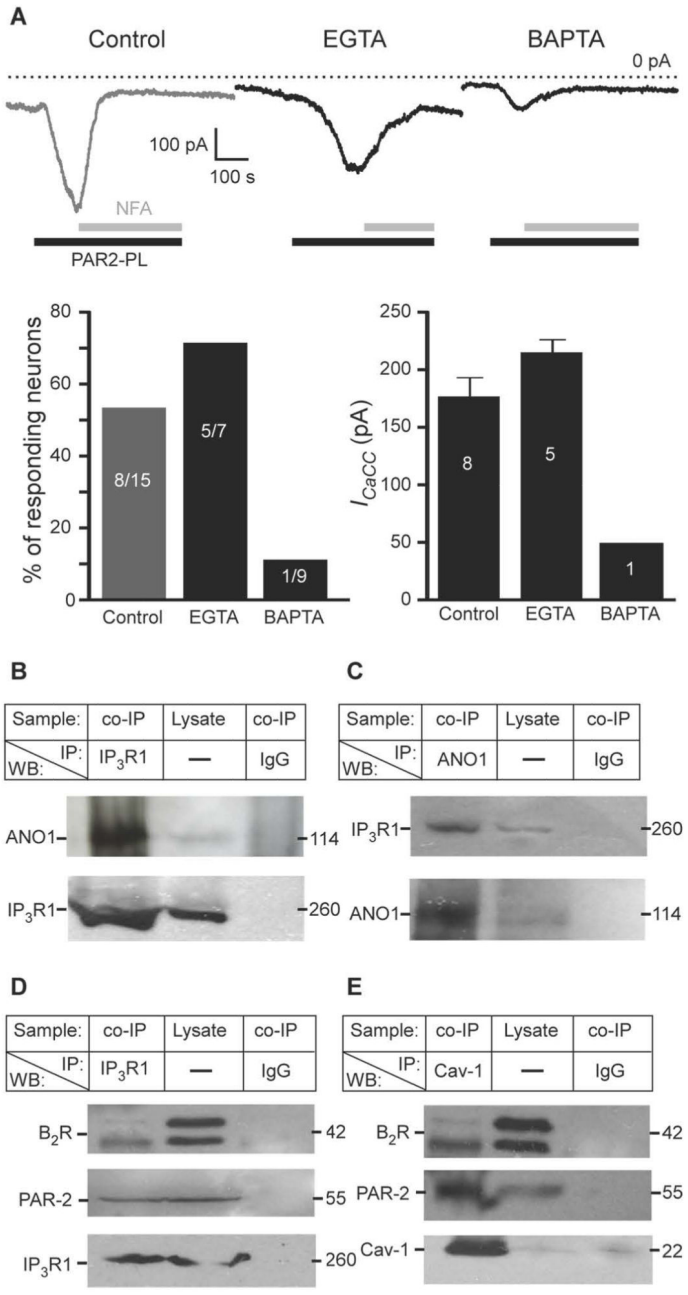

Fig. 3. ANO1 channels form signaling complexes with IP_3 receptors and GPCRs

(A) Top: Traces of inward currents measured in neurons in response to PAR-2-PL (10 μM) subjected to whole-cell dialysis with BAPTA (10 mM, 4 min) or EGTA (10 mM, 4 min) or control (no calcium chelator). Holding potential was −60 mV. Bottom: Summary and quantification of the results. **(B, C)** Immunoprecipitation of ANO1 by an antibody against IP_3R1 (B) and of IP_3R1 by an antibody against ANO1 (C) from lysates of whole DRG from rat. Control immunoprecipitations were performed using mouse or goat IgG as appropriate. IP: and WB: indicate the antibodies used for immunoprecipitation and Western blotting, respectively; co-IP, coimmunoprecipitation. **(D)** Immunoprecipitation of B_2R (upper panel)

and PAR-2 (middle panel) by an antibody against IP_3R1. Control immunoprecipitations were performed using mouse IgG. **E**, immunoprecipitation of B_2R (upper panel) and PAR-2 (middle panel) receptors by an antibody against Cav-1. Control immunoprecipitations were performed using mouse IgG. In B-E, all results shown are representative of three independent experiments and 5% of total lysate protein was used for input (Lysate).

Europe PMC Funders Author Manuscripts

Europe PMC Funders Author Manuscripts

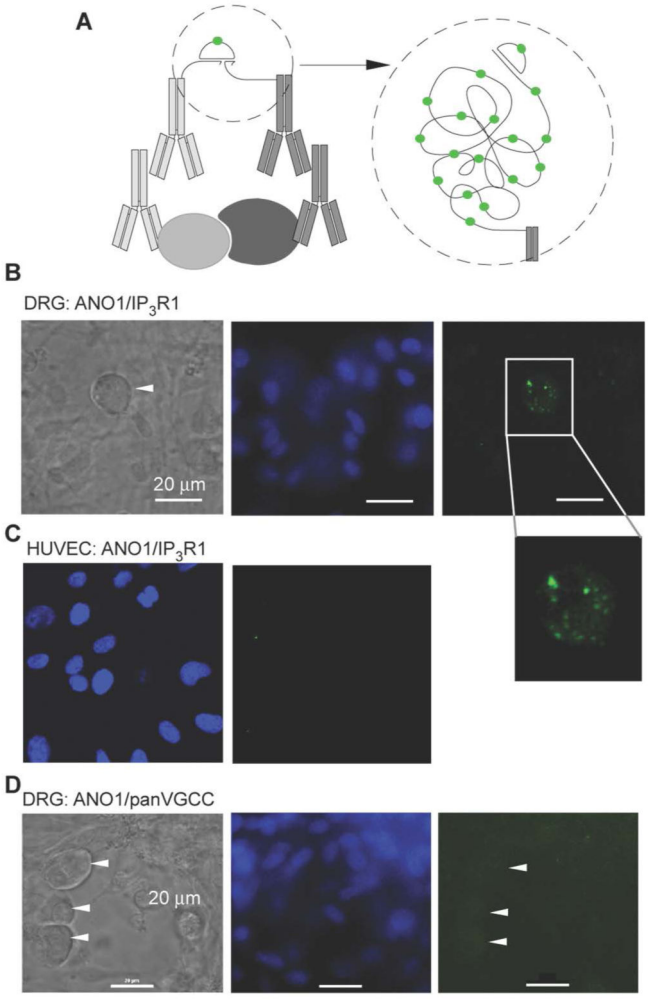

Fig. 4. PLA indicates that ANO1 and IP_3R1 are in close proximity

(A) Schematic illustrating principle of PLA. When two proteins are in close proximity, the antibodies connected to specific DNA fragments are close enough to complementary bind to a connector oligonucleotide, which then forms a circular structure amplified in a rolling cycle amplification (RCA) process. The RCA product is detected by hybridization of dye-conjugated oligonucleotides complementary to a tag sequence in the RCA product (43). **(B)** Punctate ANO1-IP_3R1 PLA signal in small-diameter DRG neuron but not in surrounding glia. Image on the left is a bright-field illumination, middle image shows DAPI staining; image on the right shows the PLA signal as detected with a 488 nM argon laser; representative of three independent preparation. **(C)** Absence of ANO1-IP_3R1 PLA signal in HUVECs (left image shows DAPI staining, right image shows PLA staining); representative of two independent preparations. (**D**) Absence of ANO1-VGCC PLA signal in DRG cultures (neurons and glia); pan-VGCC antibody was used to immunolabel VGCC; representative of two independent preparations.

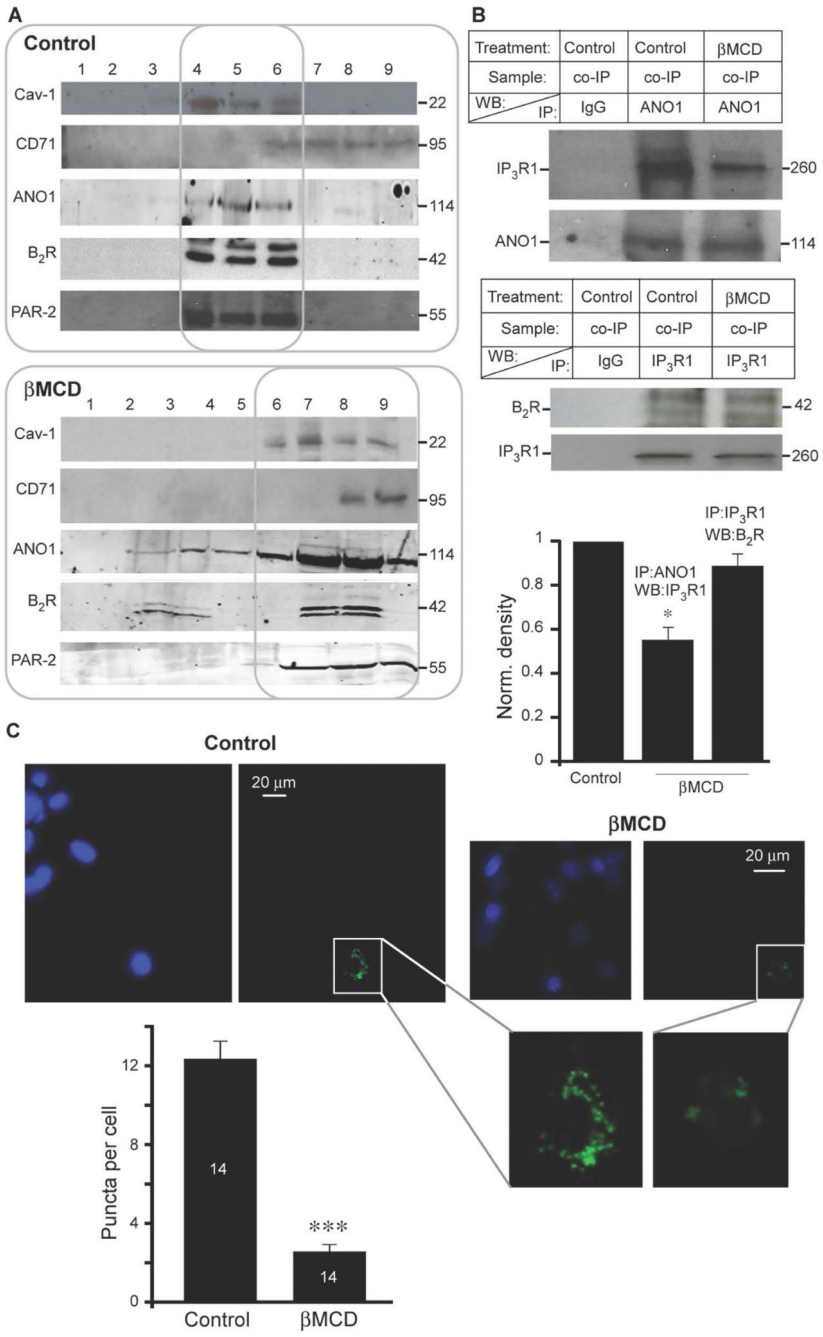

Fig. 5. ANO1 localizes to lipid rafts in DRG neurons

(A) Sucrose density gradient fractionation of detergent extracts of rat DRG immunoblotted for Cav-1 (lipid raft marker), ANO1, B_2R, PAR-2 and transferrin receptor (CD71, non-raft-localized protein) under control conditions or following cholesterol extraction of the lysates with 50 mM methyl-β-cyclodextrin (βMCD). Each experiment was repeated at least three times. **(B)** Immunoprecipitation of ANO1 (upper blot) or B_2R (lower blot) with IP_3R1 from control DRG lysate or in DRG lysate treated with βMCD. Bar chart summarizes densitometry data from three independent experiments. Mean optical densities from

identical areas around each coimmunoprecipitation band (upper blots) were normalized to the density of the corresponding WB band (lower blots); the density of the bands in βMCD-treated samples is expressed as a fraction of control. Results are representative of three or more independent experiments; * $p \leq 0.05$. **(C)** Effect of βMCD treatment on ANO1-IP_3R1 interaction detected by PLA in DRG neurons. DAPI and PLA images are shown for control and βMCD-treated cultures as indicated. The bar chart summarizes the number of puncta per PLA-positive neuron (control, n = 14; βMCD, n = 14). *** $p \leq 0.001$

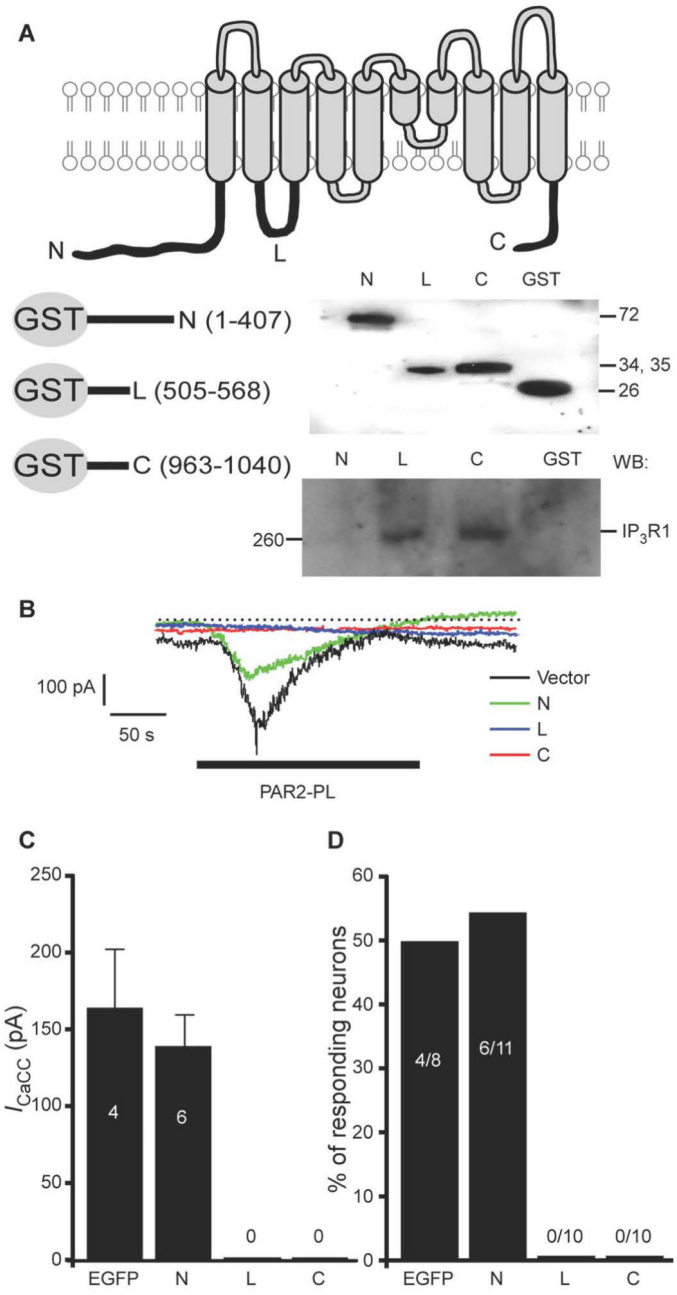

Fig. 6. ANO1 and IP_3R1 are engaged in functional interaction

(A) GST pull-down experiments. Top panel is a schematic depiction of ANO1 channel. Below left is a schematic depiction of GST-fusion proteins containing the C-terminus (residues 963-1040, 'C'), the loop between the second and third transmembrane domains (residues 505-568, 'L') and the N-terminus (residues 1-407, 'N') of ANO1. Below right: upper Western blot shows the purified GST-fusion peptides (detected with the antibody against GST); lower panel shows a pull-down experiment with the indicated peptides and IP_3R1 from the DRG lysate (detected with the antibody against IP_3R1). All results shown are representative of three independent experiments. (**B)** The effect of the three cytosolic

domains of ANO1 on PAR2-PL-induced inward currents in DRG neurons. Each ANO1 cytosolic domain was individually overexpressed in DRG neurons and inward current was tested by patch clamp. Traces are representative recordings from cells transfected with the indicated constructs. Vector is EGFP only. Periods of PAR2-PL (10 μM) application are indicated by black bar. (**C, D**) Bar charts summarizing the current amplitudes (C) and proportions of the neurons displaying inward current (D) in the indicated neuron groups.

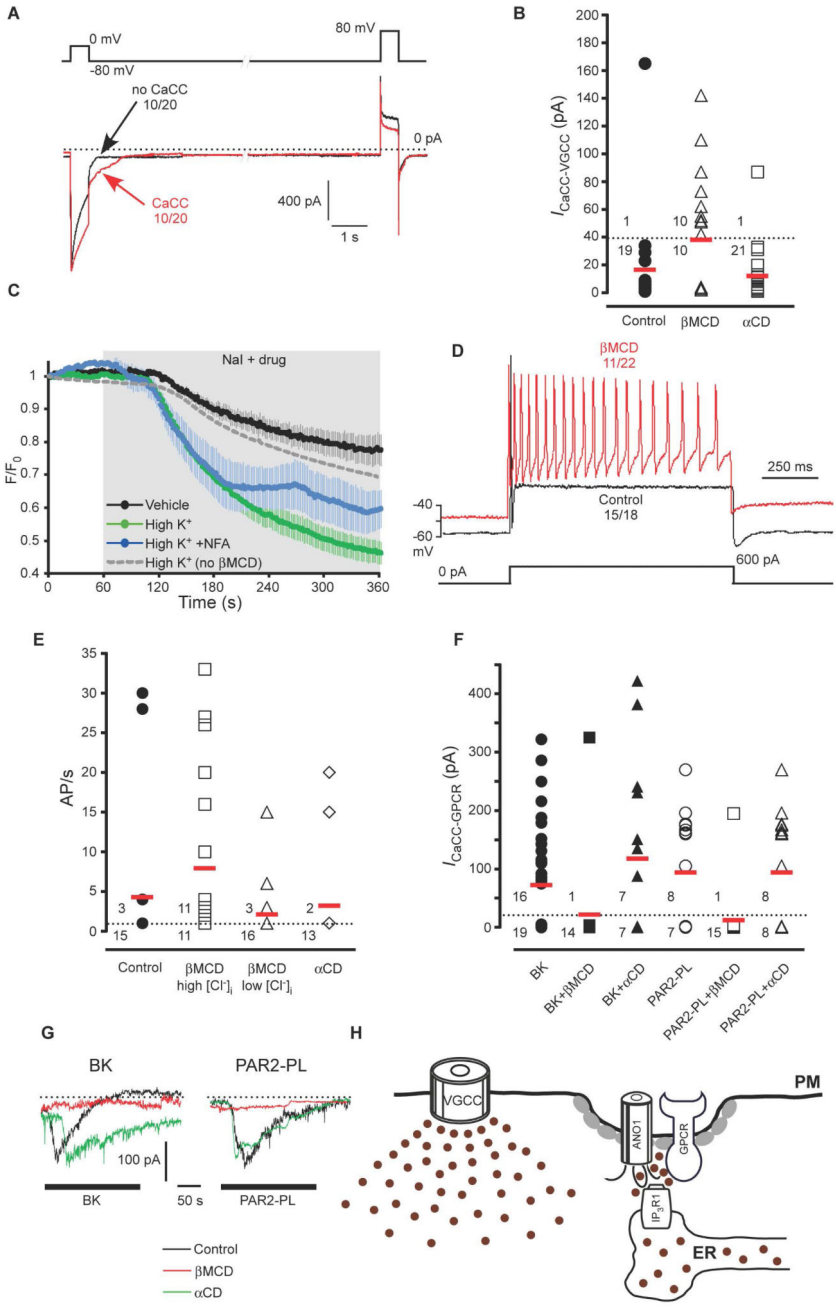

Fig. 7. Disruption of ANO1-containing complexes results in coupling of CaCC activity to 'global' Ca^{2+} elevations and overexcitable neurons

(A) Whole cell patch-clamp experiments showing effect of treatment of cultured DRG neurons with 10 mM βMCD for 30 min on inward tail current. Voltage protocol and labelling as in Fig. 1A. **(B)** Summary for control, βMCD, and αCD (10 mM, 30 min) experiments like those shown in (A) for βMCD-treated neurons. $I_{CaCC-VGCC}$ was calculated as a difference in peak tail current amplitudes after the depolarizing pulses with and without Ca^{2+} influx; neurons were considered as not displaying activation of CaCC by VGCC when the resulting amplitude was below 40 pA. Red horizontal bars represent mean values of all

neurons tested in each group. Numerals above and below the dotted line represent number of neurons with and without VGCC-induced CaCC, respectively. **(C)** Effect of βMCD treatment on I^- influx induced by depolarization with 50 mM KCl in DRG neurons. Averaged time courses of normalized fluorescence (F/F_0) of H148Q/I152L EYFP-transfected neurons perfused with 30 mM NaI-containing extracellular solution either alone (vehicle, n = 7) or in neurons treated with βMCD (10 mM, 30 min) and then stimulated with 50 mM KCl (High K^+, n = 10) or 50 mM KCl and NFA (100 μm) (High K^+ +NFA, n=5). The time of application of NaI and the depolarizing stimulus is indicated by the shaded area. Dotted grey line represent mean data for the effect of 50 mM KCl in control (βMCD untreated) neurons; taken from the Fig. 2B for comparison. (**D)** Current clamp experiments showing action potentials of control DRG neurons or neurons treated with βMCD in response to injection of a 600 pA depolarizing current pulse (depicted under the traces). (**E)** Summary for the experiments like those shown in (D); labelling as in (B) for neurons exposed to βMCD in the presence of high or low intracellular Cl^- or in neurons exposed to αCD. (**F)** Summary of the effects of βMCD or αCD treatment on the GPCR-induced CaCC. (**G**) Exemplary current traces from the experiments summarized in (F). (**H)** Simplified scheme of the proposed juxtamembrane arrangements within an ANO1-containing signaling microdomain. Gray ovals represent Cav-1.

Europe PMC Funders Author Manuscripts

Table 1

Summary of the effects of cholesterol extraction on the coupling of CaCC activity to BK- and PAR-2-induced Ca^{2+} release and to VGCC-mediated Ca^{2+} influx

Numbers represent amount of neurons displaying a given property from the total amount of neurons tested for each condition. Significant differences based on χ^2 with $p < 0.05$ are indicated. N/A, not analyzed

Property:	**Condition:**	**No treatment (Control)**	**βMCD**	**αCD**
BK-induced cytosolic Ca^{2+} transients		18/31	13/31	N/A
BK-induced CaCC current		16/35	1/15*	7/14
PAR2-PL-induced CaCC current		8/15	1/16*	8/16
CaCC tail current after VGCC activation		1/20	10/20*	1/21$
Multiple AP firing			High $[Cl^-]_i$	Low$[Cl^-]_i$
		3/18	11/22*	3/19# 2/15&

*significantly different from control;

$significantly different from βMCD;

#significantly different from high $[Cl^-]_i$;

&significantly different from βMCD with high $[Cl^-]_i$